Journal of Catalysis **184,** 491–498 (1999)
Article ID jcat.1999.2454, available online at http://www.idealibrary.com on IDEAL®

The Origin of SO_2 Promotion of Propane Oxidation over Pt/Al_2O_3 Catalysts

Adam F. Lee,*[,1] Karen Wilson,*[,2] Richard M. Lambert,*[,3] Carolyn P. Hubbard,† Ronald G. Hurley,† Robert W. McCabe,† and Haren S. Gandhi†

*Department of Chemistry, University of Cambridge, Cambridge CB2 1EW, England; and †Ford Research Laboratory, Ford Motor Co., MD 3179, Dearborn, Michigan 48121-2053
E-mail: RML1@cam.ac.uk

Received November 17, 1998; revised February 9, 1999; accepted February 10, 1999

XAFS, XRD, and TEM measurements on dispersed Pt/Al_2O_3 catalysts have elucidated the promotional effect of SO_2 in propane oxidation over these systems. At low loadings (0.05 wt%), Pt/Al_2O_3 catalysts initially contain small (<20 Å) stoichiometric β-PtO_2 particles. Catalyst sulphation is accompanied by reduction and concomitant sintering of these oxidic particles, resulting in metallic Pt clusters exhibiting similar structural and reactive properties to their counterparts formed at higher loading (9 wt%). The formation of stable SO_4 species on both alumina support and on the Pt surface facilitates the dissociative chemisorption of propane onto both support and metal. Evidence is presented for the role of interfacial sulphate in the activation and subsequent oxidation of propane *via* a bifunctional mechanism.

INTRODUCTION

By virtue of its application in a number of important fields including automotive pollution control and hydrocarbon reformation, Pt/Al_2O_3 is amongst the most widespread of catalytic systems in commercial use today (1). However, despite years of intensive study, aspects of the complex interdependent interactions between Pt–alumina and poison/promoter species remain contentious. In particular the role of S-containing molecules in modifiying the catalytic oxidation activity of Pt/Al_2O_3 catalysts is unclear. As early as 1979 Sadowski and Treibmann first reported that exposure to SO_2 irreversibly enhanced the catalytic oxidation of *n*-alkanes by Pt (2). Subsequent studies by Gandhi *et al.* found that inclusion of trace SO_2 in simulated car exhaust feedstreams poisoned the Pt/Al_2O_3 catalysed oxidation of propene and carbon monoxide but promoted the oxidation of propane (3). Similar rate enhancements are observed following sulphation by 1.1 N H_2SO_4 or exposure to SO_2/O_2 mixtures (4), and SO_2-promoted propane combustion is also reported over the modern three-way catalyst (5). These reactions are directly relevant to the control of unburnt hydrocarbon emissions from automotive sources, which legislation dictates must be fully combusted to CO_2 (6). Recent research and development efforts focused at emissions control for both lean-burn gasoline and diesel vehicles have refocused attention on the role of SO_2 in reactions of both hydrocarbons and nitrogen oxides (7). Under lean-burn conditions vehicles can run for extended periods at low temperatures with consequent accumulation of high sulphate levels. This is especially true of advanced NO_x trapping systems wherein Pt/Al_2O_3 oxidises NO to NO_2 for subsequent nitrate storage.

Our previous research on model $Al_2O_3/Pt(111)$ single-crystal systems under ultra-high vacuum (UHV) conditions revealed the importance of both active phase (8) and alumina sulphation in facilitating propane chemisorption and subsequent combustion (9).

Here we investigate the extent to which our single-crystal findings are pertinent to practical highly dispersed Pt/Al_2O_3 catalysts. We show that while the principal promotional phenomena identified with model catalyst systems do indeed transfer across the "structure and pressure gap." The key role of SO_2 in the case of supported catalysts involves sulphate-induced simultaneous reduction and sintering of highly dispersed oxidised Pt particles, present within fresh catalysts under normal high-pressure operating conditions. We are thus able to rationalise the original microreactor study of Gandhi and co-workers.

EXPERIMENTAL METHODS

Model catalyst studies on Pt(111) and $Al_2O_3/Pt(111)$ single-crystal surfaces were performed in a UHV system described previously (10), operated at a base pressure of

[1] Present Address: Department of Chemistry, University of Hull, Hull HU6 7RX, England.
[2] Present Address: Department of Chemistry, University of York, York YO1 5DD, England.
[3] Corresponding author: telephone, +44 1223 336467; fax, +44 1223 336362.

0021-9517/99 $30.00

1×10^{-10} Torr. γ-Al_2O_3 surfaces were prepared by oxidation and annealing of metallic Al films deposited onto Pt(111) in an O_2 background pressure of 1×10^{-6} Torr as reported previously (9). Temperature-programmed reaction measurements were acquired with a heating rate of 10 K s^{-1} using a multiplexed quadrupole mass spectrometer for the detection of desorbing species.

Ex-situ XAFS (X-ray absorption fine structure) experiments were performed on the Ultra-Dilute Spectroscopy Station 16.5 of the Daresbury SRS facility, using a Si(311) double-crystal monochromator with a beam current/energy of 150 mA/2 GeV. The Pt/Al_2O_3 samples were prepared by incipient wetness from a hexachloroplatinic acid precursor, with Pt loadings of 0.05, 3, and 9 wt% as determined by ICP-MS. Subsequent catalyst sulfation was performed at 673 K for 1 hr using a 1 : 1 SO_2 : O_2 gas mix at 1 bar (10 ml min^{-1}). Prior to XAFS measurements all catalysts were reduced at 673 K for 2 hr and then re-oxidised at 773 K for 2 hr to mirror the pretreatments used in earlier reactivity studies (4). Samples were then pressed into self-supporting discs. Pt L_{III}-edge (11.5 keV) XAFS of the 0.05 and 3% catalysts were acquired in fluorescence mode at 300 K in air, using a three-element solid-state multichannel detector mounted in the horizontal plane. XAFS of the 9% catalyst and an 8 μm Pt foil reference were taken in transmission. Extended X-ray absorption fine structure (EXAFS) analysis was undertaken using the Daresbury EXBROOK and EXCURV92 packages for background subtraction, phaseshift determination, and iterative least-squares fitting procedures, respectively. Total surface areas of fresh and sulphated catalysts were determined by the BET (N_2) method using a Micromeritics 2700 analyser. X-ray diffraction (XRD) spectra of fresh and sulphated catalysts were acquired with a Siemens D500 diffractometer for $2\theta = 20$–100° in increments of 0.2°, while particle size distributions were determined using a JEOL transmission electron microscope (TEM).

RESULTS AND DISCUSSION

The structural and electronic properties of a range of unsulphated (fresh) and sulphated (exposed to SO_2/O_2) Pt/Al_2O_3 catalysts were examined in order to identify differences and correlate these with the associated promotion of propane catalytic oxidation. X-ray absorption spectroscopy proved invaluable, being the only nondestructive probe available for characterising the structure and oxidation state of the very small particles central to this study. CO and H_2 chemisorption are ineffective for such high dispersion catalysts where the adsorbate : Pt stoichiometry is unknown and frequently yields dispersions greater than unity (11). It was also important to avoid chemical reduction of any surface sulphate/oxide species present within the samples.

The presence of crystalline phases within fresh and sulphated Pt/Al_2O_3 catalysts was investigated by XRD. The diffraction patterns for the 0.05% loading catalysts are dominated by reflections arising from the γ-alumina support phase in the fresh sample and those from mixed aluminium sulphate phases in the sulphated sample. Additional weak diffraction features suggest the presence of trace platinum oxide phases; however, no peaks characteristic of Pt metal are apparent in either fresh or sulphated samples. Figure 1 illustrates spectra obtained from the 3% catalyst prior to (fresh) and after sulphation. Diffraction data for the fresh 3% catalyst resembles that of the lower loading sample, predominantly exhibiting reflections from the alumina

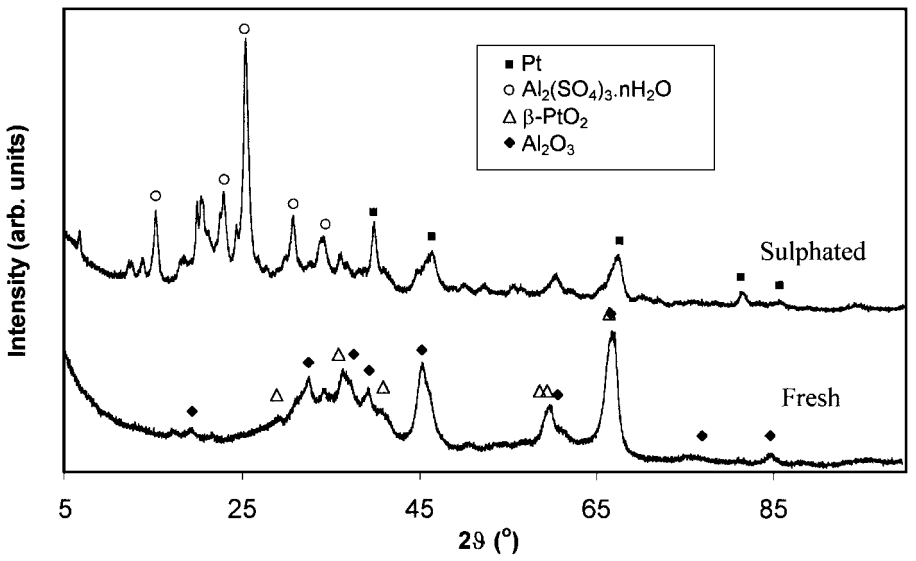

FIG. 1. X-ray diffractograms of fresh and sulphated 3 wt% Pt/Al_2O_3 catalysts.

support. Weaker peaks at 30, 38, and 56° are attributed to a PtO_2 phase (12), although the presence of other minority platinum oxide phases cannot be discounted. Sulphation of the 3% Pt/Al_2O_3 catalyst results in attenuation of the alumina support phase and the appearance of intense peaks arising from mixed aluminium sulphate hydrates (principally $Al_2(SO_4)_3 \cdot 16H_2O$ and $Al_2(SO_4)_3 \cdot 14H_2O$ (13)). Deng *et al.* have also reported bulk alumina sulphation for commercial Pt/Al_2O_3 catalysts exposed to sulphur under weakly oxidising atmospheres (14). Reflections attributable to a metallic fcc Pt phase also emerge at 39.4, 46.4, 67.7, 81.3, and 85.7° following sulphation (15). These metallic features are clearly resolved in the fresh 9% catalyst, wherein sulphation likewise promotes their growth and narrowing.

Particle size determination based on the Pt(111) reflection using the Debye–Scherrer equation yields volume-averaged Pt crystallite diameters of 100 and 200 Å for the 3 and 9% sulphated catalysts, respectively. The absence of assignable Pt-derived reflections prohibited similar analysis for the lowest loading samples; however, TEM measurements provide clear evidence for the expected increase in Pt particle size with metal loading and furthermore demonstrate sulphate-induced sintering of Pt on alumina. Figure 2 presents the particle size distributions derived from TEM. As with XRD, particle size analysis of the fresh 0.05% Pt/Al_2O_3 catalyst was beyond our instrumental detection limit; however, following sulphation a narrow distribution of Pt particles, peaked ~40 Å diameter, was observed. Many of these particles exhibit regular morphologies, characteristic of cubeoctahedral and tetragonal metal particles. A similar trend is apparent for the 3% catalysts, which show a narrow distribution peaked ~50 Å in the fresh sample, broadening after sulphation to a greater mean diameter of ~100 Å. XRD and TEM data confirm sulphation sinters the large Pt crystallites present in the fresh 9% Pt/Al_2O_3 sample, narrowing the size distribution and increasing the mean Pt particle diameter from ~150 to 200 Å.

Table 1 shows BET surface areas determined for the fresh and sulphated catalysts. The surface areas of the fresh samples are all close to those of the alumina support at ~95 $m^2 g^{-1}$. However, following sulphation, all Pt/Al_2O_3 samples display a significant loss of between 20 and 35% of their fresh surface areas. The loss of catalyst surface area is consistent with the crystallisation of amorphous alumina as aluminium sulphate hydrates and is greatest for the higher loading samples, which is supportive of Pt-promoted alumina sulphation (14). These changes cannot be accounted for by simple loss of total metal area of the fresh catalysts (as determined by H_2 titration of *reduced* samples (4)), which would only account for a reduction of ~5 $m^2 g^{-1}$.

TABLE 1

BET Surface Areas of Fresh and Sulphated Pt/Al_2O_3 Catalysts

Pt/Al_2O_3 sample	Surface area/$m^2 g^{-1}$ (±1)
0.05 wt%–calcined	100
0.05 wt%–sulphated	74
3 wt%–calcined	96
3 wt%–sulphated	65
9 wt%–calcined	91
9 wt%–sulphated	58

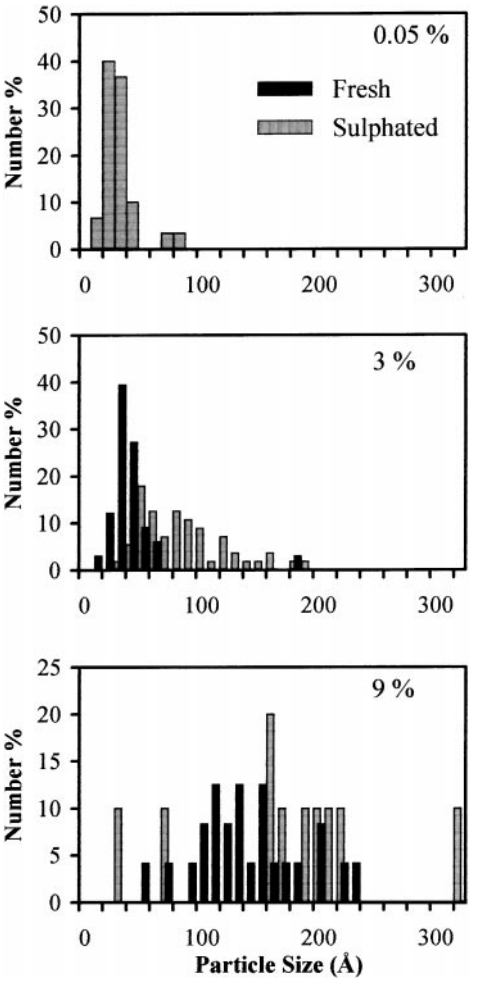

FIG. 2. Transmission electron micrographs of fresh and sulphated Pt/Al_2O_3 catalysts.

In order to elucidate the detailed structural changes associated with sintering of the Pt particles, XAFS data on the Pt L_{III}-edge were acquired *ex situ* on both fresh and sulphated Pt/Al_2O_3 catalysts. The resulting raw XAFS spectra are shown in Figs. 3a and b, respectively, together with a reference Pt foil, normalised with respect to their white-line intensities (edge-step heights). For the fresh samples, the white-line relative intensity clearly decreases with increasing Pt loading while the range of EXAFS oscillations simultaneously extends, such that the XAFS of the 9% Pt/Al_2O_3 catalyst closely resembles that of the Pt foil. These trends coincide with the emergence of new structure in the near-edge (XANES) region, associated with allowed transitions

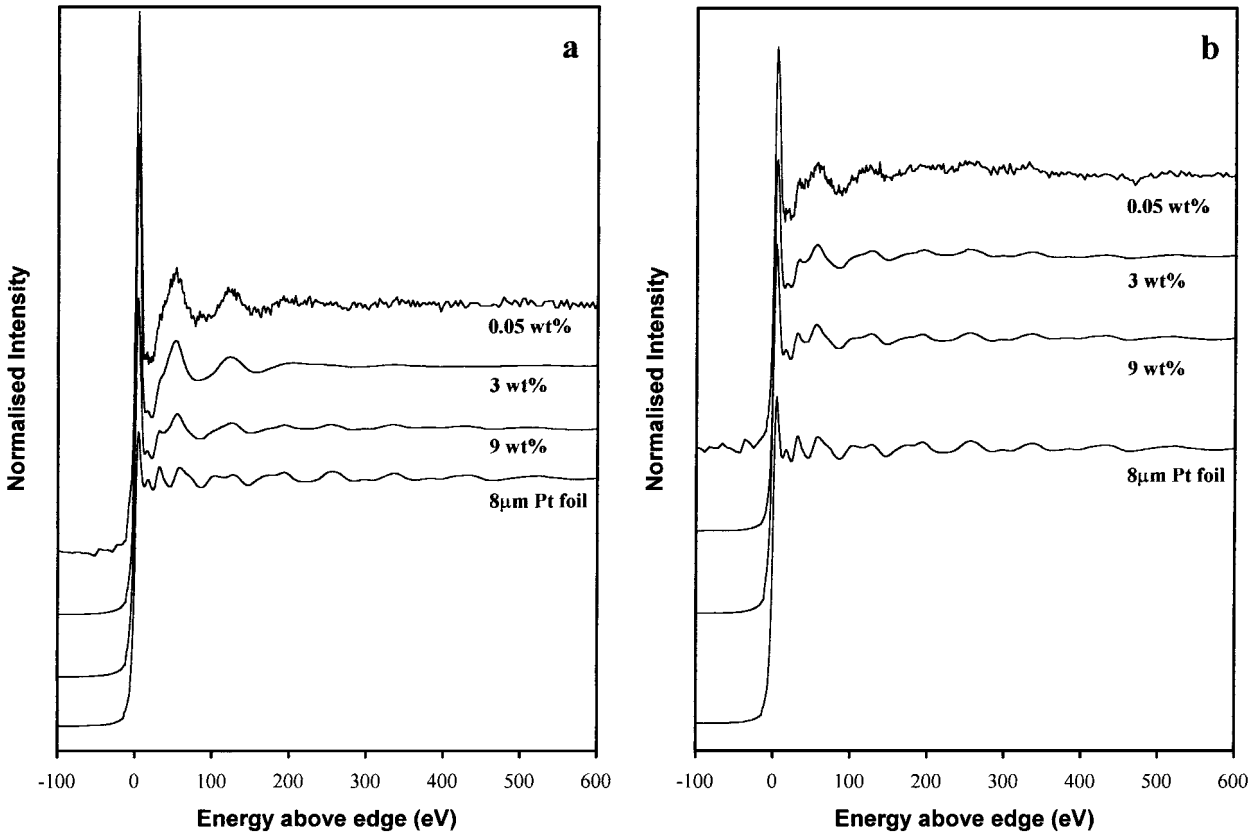

FIG. 3. Normalised, raw Pt L_{III}-edge XAFS spectra of (a) fresh and (b) sulphated Pt/Al_2O_3 catalysts. For comparison, 8 μm Pt foil spectrum is shown.

from bound Pt $2p_{3/2}$ to quasibound vacant states (of principally *d* character) above the Fermi level (16). The XANES region thus reflects the Pt band structure, and in turn the influence of compound formation on the charge distribution on Pt atoms within the catalysts (17). In particular, a strong white-line is indicative of a high probability for bound electronic transitions between the Pt $2p_{3/2} \rightarrow 5d_{5/2}$ bands, and thus significant Pt 5*d* vacancies. Bulk metallic Pt possesses only ~0.3 *d* holes/atom (18) and hence does not exhibit the strong white-lines characteristic of Pt coordinated to electronegative moieties.

Catalyst sulphation (Fig. 3b) reduces the Pt loading dependence apparent in the fresh Pt/Al_2O_3 catalyst XAFS, reducing the white-line intensities of the 0.05 and 3% samples, and promoting the emergence of XANES features representative of their higher loading and bulk Pt counterparts. The simplest interpretation of these changes is in terms of sulphate-induced simultaneous reduction and growth of the supported Pt phase initially present within the fresh 0.05 and 3% catalysts, producing extended metallic Pt particles with a similar electronic structure to that of bulk Pt metal.

The corresponding background-subtracted, k^3-weighted EXAFS (χ) data for the fresh and sulphated Pt/Al_2O_3 catalysts are shown in Figs. 4a and b, respectively. Due to the poorer signal : noise ratio inherent for such a low Pt loading, EXAFS of the 0.05% Pt/Al_2O_3 catalyst are Fourier-transformed between 2 and 15 $Å^{-1}$ and filtered to remove high-frequency noise by back-transformation of the resultant pseudo-radial distribution function between 1 and 4 Å. Similarities between the data for the 9% catalyst and bulk Pt metal (themselves distinct from the 0.05 and 3% EXAFS) are again evident. This confirms expectations that large supported Pt particles, obtained using high metal loadings, recover the local structural properties of bulk Pt (19–21). Sulphation removes both the metal loading dependence seen in the EXAFS of the fresh samples and differences between the catalysts and the Pt foil. This is again indicative of a sulphate-induced transformation of Pt in the low loading catalysts into an extended metallic phase.

Figures 5a and b show the associated pseudo-radial distribution functions for fresh and sulphated Pt/Al_2O_3 samples, and the fitted parameters are presented in Table 2. Fourier filtration was only applied to EXAFS data from the 0.05% samples. Good fits to the 0.05 and 3% fresh catalysts could only be obtained for a first coordination shell containing oxygen nearest-neighbours, with a Pt–O separation

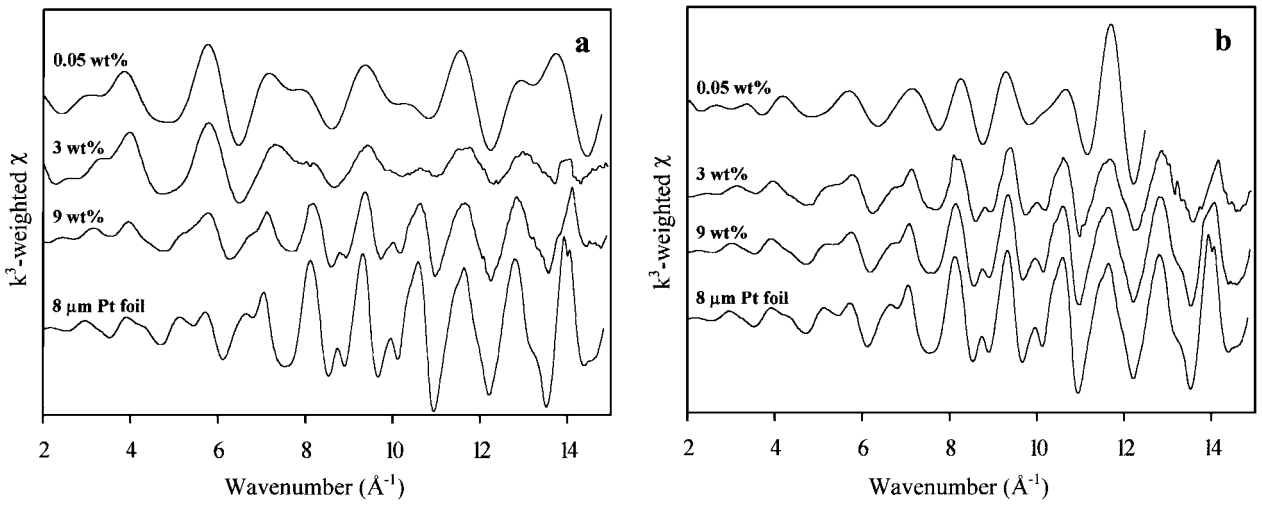

FIG. 4. Pt L_{III}-edge k^3-weighted raw EXAFS of (a) fresh and (b) sulphated Pt/Al_2O_3 catalysts. (The 0.05 wt% sample data have been Fourier-filtered.) For comparison 8 μm Pt foil spectrum is shown.

of ~2.0 Å, together with a next-nearest neighbour Pt–Pt scattering pair at 2.75 Å. In contrast, EXAFS of both the fresh and sulphated 9% catalysts exhibit only Pt–Pt scattering contributions, extending over four local coordination shells, akin to the Pt foil. Increased Pt loading therefore correlates with a reduced Pt coordination to oxygen and concomitant rise in bulk Pt-like character for the fresh catalysts, together with a rise in the total Pt local coordination number. The fitted parameters for the 0.05% fresh catalyst are consistent with those expected for the PtO_2 phase (19, 22) observed by XRD (Fig. 1), with a first coordination shell of six O atoms, and a second shell of approximately three Pt neighbours. Although the Pt–Pt separation of 2.75 Å is significantly shorter than the 3.0 Å anticipated for bulk β-PtO_2, such contractions are common for small, dispersed Pt particles wherein large structural distortions are reported (23). The propensity for oxidation of highly dispersed Pt particles on oxide supports, notably alumina and silica, is well documented (24–26), particularly for particles with diameters <20 Å (20). Accurate estimates of Pt particle size within the fresh 0.05% Pt/Al_2O_3 catalyst employed in this study were not possible due to the very low Pt concentration. However, in view of our XRD and TEM instrumental detection limits of ~15–20 Å, and the previously reported unity dispersion of this sample (4), we surmise that the PtO_2 particles are indeed <20 Å. It is thus clear that following conventional impregnation and reduction/calcination pretreatments, low-loading Pt/Al_2O_3 catalysts comprise small, highly dispersed oxidic Pt particles, whereas their higher metal loading analogues contain large metallic Pt particles.

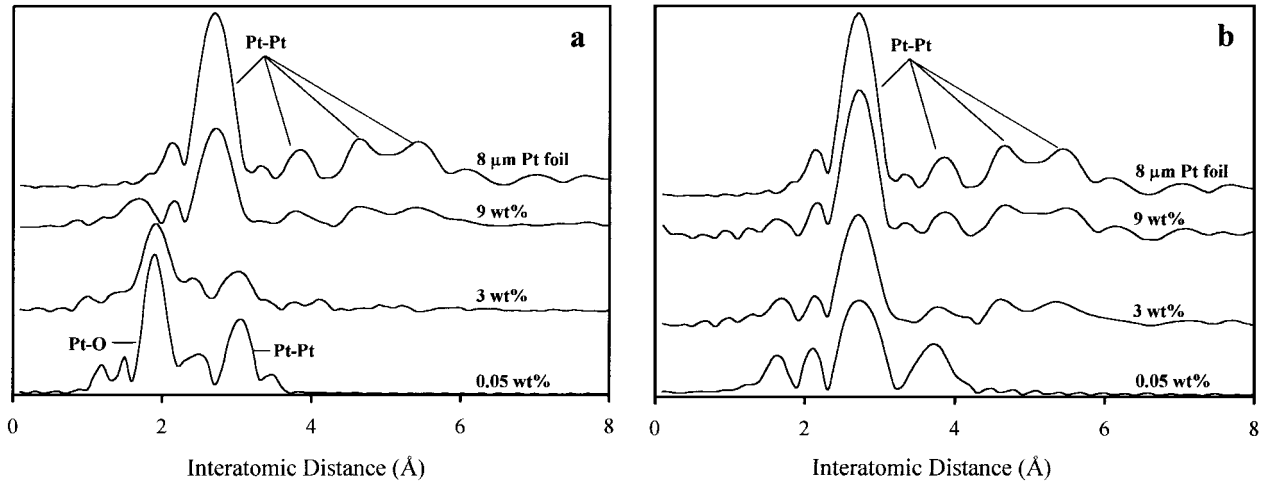

FIG. 5. Pt L_{III}-edge pseudo radial distribution functions of (a) fresh and (b) sulphated Pt/Al_2O_3 catalysts. (The 0.05 wt% sample data have been Fourier-filtered.) For comparison, 8 μm Pt foil spectrum is shown.

TABLE 2

Structural Parameters Derived from Fitted EXAFS Data of Fresh and Sulphated Pt/Al_2O_3 Catalysts

		Fresh			Sulphated		
Parameter	Pt foil	0.05%	3%	9%	0.05%	3%	9%
CN^1_{Pt-O}	—	6	4.2	—	—	—	—
CN^1_{Pt-Pt}	12	3.6	4.4	7.5	7.7	8.7	9.2
CN^2_{Pt-Pt}	6	—	—	4.5	5.7	4.9	4.1
r^1_{Pt-O}/Å	—	1.98	1.99	—	—	—	—
r^1_{Pt-Pt}/Å	2.77	2.76	2.75	2.76	2.76	2.76	2.77
r^2_{Pt-Pt}/Å	3.92	—	—	3.91	3.85	3.89	3.92
σ^1_{Pt-O}	—	0.007	0.008	—	—	—	—
σ^1_{Pt-Pt}	0.011	0.009	0.017	0.012	0.009	0.013	0.01
σ^2_{Pt-Pt}	0.013	—	—	0.019	0.007	0.019	0.013

After sulphation the Pt–O shell present in the fresh 0.05 and 3% Pt/Al_2O_3 catalysts is absent, with evidence only of coordination to Pt neighbours, indicative of particle reduction. Sulphation also increases the total local coordination of Pt atoms within all three samples, suggesting the formation of more extended structures, and thus of Pt particle growth. Such trends are consistent with both our XRD and TEM measurements, which demonstrate SO_2-promoted Pt metal crystallisation, and the sintering of pre-existing small Pt metal particles, respectively (Figs. 1 and 2).

Additional XPS measurements performed in Cambridge on the dispersed Pt/Al_2O_3 catalysts proved unhelpful due to the intense Al 2*p* XP signal which obscures the principal Pt 4*f* transition (9). Although the weaker Pt 4*d* transition could be detected for the highest loading catalysts, the low signal prohibited any peak analysis. However, in accordance with the XRD data presented in Fig. 1, a strong S 2*p* feature was observed on all sulphated catalysts at 167 eV binding energy (referenced with respect to an Au strip), characteristic of a surface sulphoxy species (27).

The preceding structural properties, and their impact on Pt/Al_2O_3-catalysed propane oxidation, may be rationalised as follows.

The fresh Pt/Al_2O_3 catalysts used in this and many other studies are usually activated by a high-temperature reduction/oxidation pretreatment, nominally generating clean, reduced Pt particles on a stoichiometric oxide support. However, as observed in other work, such pretreatments often yield oxidic rather than metallic Pt particles on alumina supports, particularly where low metal loadings, i.e., highly dispersed particles, are used (20, 25, 26). High-temperature oxidation ($\sim$500°C) of chlorine-containing Pt catalysts is known to promote Pt redispersion, possibly via oxichloride formation (28, 29). Although the thermodynamic stability of bulk PtO_2 is significantly lower than that of other bulk platinum group metal oxides, the formation of small Pt particles may facilitate their complete oxidation via two factors. First, such small Pt particles experience a greater interaction with interfacial oxygen than larger particles. Second, surface energy considerations favour the formation of PtO_x surfaces over Pt metal (30). Under extreme conditions, where an entire platinum crystallite is oxidised, Ruckenstein and Chu proposed the substrate–crystallite interfacial tension may drop sufficiently that pseudo-2D platinum oxide particles are formed that completely wet alumina supports (31).

The origin of the strong structure sensitivity previously reported for propane oxidation over these unsulphated catalysts (3) is now clear. High Pt loading (low dispersion) catalysts, comprising large *metallic* Pt crystallites, exhibit the highest activities since they provide active sites for both oxygen dissociation and heterolytic C–H bond scission, widely held as the rate-determining step in alkane activation. [As discussed by Burch *et al.* (32), dissociative oxygen chemisorption over Pt metal surfaces results in a partially oxidised surface exposing both $Pt^{\delta+}$ and comparatively weakly bound $O_a^{\delta-}$ sites efficient in polarising C–H bonds. However fully oxidised PGM surfaces are known to actually inhibit combustion. Xu and Friend have shown surface oxygen inhibits allylic C–H cleavage in propene combustion over Rh(111) surfaces (33), thus preventing propylidyne formation and subsequent total oxidation pathways.] Conversely despite their higher surface area, the small platinum oxide particles present in low-loading Pt/Al_2O_3 catalysts thus exhibit poor alkane oxidation performance. These conclusions are supported by kinetic studies which reveal that the rise in propane oxidation rate with Pt loading is not accompanied by a change in activation energy (4, 11, 25, 35), suggesting that only the active site density and not the nature of reaction centres varies with Pt dispersion. Hence we propose that propane oxidation cannot occur on highly dispersed PtO_x particles, and the limited activity observed for low-loading Pt/Al_2O_3 catalysts arises from the presence of a few larger metallic Pt particles, an idea first advanced by Otto *et al.* (34). *The structure sensitivity observed for propane oxidation over Pt/Al_2O_3 therefore appears to be associated with the phase transformation from PtO_2 to Pt and not with the size of available Pt ensembles.*

Our results suggest that sulphation promotes propane oxidation over Pt/Al_2O_3 catalysts in three distinct ways. First, sulphation modifies the alumina support, generating crystalline aluminium sulphate and associated surface sulphoxy groups. Our earlier work using model γ-Al_2O_3/Pt(111) surfaces demonstrates that sulphated alumina surfaces greatly enhance the dissociative chemisorption and subsequent oxidation of propane on neighbouring partially oxidised Pt sites (8, 9). It has been postulated that heterolytic C–H bond scission yields an alkyl sulphate intermediate prior to the chemisorption of alkyl fragments onto Pt (35). Since the intrinsic sticking probability of alkanes on low-index

Pt single-crystal surfaces is very low (36), support sulphation may act to increase the surface concentration of hydrocarbon species resulting from H abstraction, and thus oxidation activity relative to that of the fresh Pt/Al_2O_3 catalysts. Previous IR data (3, 44) taken with dispersed fresh and sulphated Pt/Al_2O_3 catalysts exposed to a propane reaction mixture supports this prediction. Adsorbed hydrocarbon species are only observed over the sulphated catalysts. Second, our UHV studies also show that surface sulphate enhances dissociative propane chemisorption over Pt surfaces in the absence of any alumina (8). Hence although the stability of surface sulphate on metallic Pt clusters is much lower than that of the aluminium sulphate support phase (37), catalyst sulphation may also facilitate a direct, low-temperature route for propane adsorption onto the surface of sulphated Pt clusters. We believe both these factors contribute to the small enhancement in oxidation rate ($\Delta T_{50} = -50$ K) observed over high-loading (9 wt%) Pt/Al_2O_3 catalysts. Third, we have demonstrated the sulphate-induced reduction and sintering of highly dispersed platinum oxide particles, predominant for low-loading (0.05 and 3 wt%) Pt/Al_2O_3 catalysts. The resultant large metallic platinum particles exhibit higher activities towards propane activation ($\Delta T_{50} = -140$ K), for reasons discussed above. Hence the principal promotional effect of SO_2 upon low-loading Pt/Al_2O_3 catalysts is to reduce PtO_2 to Pt, eliminating structural differences with their higher loading counterparts, thereby lifting the dependence of propane oxidation activity on Pt concentration found in unsulphated samples.

Irreversible sintering of Pt particles in Pt/Al_2O_3 (38) and Pt/BaK-LTL zeolites (39) has been reported following exposure to H_2S. The agglomeration of small ($\sim$10 Å) Pt particles was attributed to preferential H_2S adsorption at the Pt–O–Al/Ba interface, weakening the Pt–O interaction and promoting the migration and agglomeration of metallic Pt. We propose that Pt reduction and sintering proceeds by a similar mechanism over our catalysts. Exposure of pre-oxidised Pt/Al_2O_3 catalysts to SO_2 results in preferential reaction of SO_2 with weakly bound oxygen at the Pt-O-Al interface, promoting interfacial sulphate formation and concomitant reduction of Pt. This reaction may also be facilitated by the associated exothermic Pt/Al surface alloying at the resultant Pt–AlO_x interface. Our single-crystal studies have demonstrated that this is an efficient process even at 300 K (40). Pt/Al alloying has also been observed for dispersed Pt/Al_2O_3 catalysts under reducing environments (41, 42). Reduction to the metallic state raises the surface energy of the Pt particles destabilisng highly dispersed clusters, and leading to irreversible sintering and promotion of catalytic propane activation. Otto *et al.* have observed similar *reversible* H_2-induced sintering and catalytic promotion phenomena (34).

Our UHV measurements show that interfacial sulphate also plays a role in promoting bifunctional catalytic oxidation of propane. Figure 6 shows the integrated yield of combustion products arising from the temperature-programmed oxidation of propane over sulphated Al_2O_3/Pt(111) surfaces as a function of alumina overlayer coverage. The inset shows the associated typical desorption profile of SO_2 (arising from surface SO_4 decomposition), which exhibits two desorption states. The low-temperature desorption is observed from clean Pt(111) surfaces exposed to SO_2, O_2, and propane, and we associate this state with sulphate decomposition and desorption from bare Pt metal sites (43). The high-temperature peak is only observed from alumina-precovered Pt(111) surfaces exposed to SO_2, O_2 and propane, and the integrated intensity of this state is also plotted in Fig. 6. The coverage dependence of the strongly bound surface sulphate displays a volcano dependence on alumina film thickness, peaking at $\sim$1 ML (monolayer). This alumina coverage does not correspond to monolayer completion, due to the formation of three-dimensional Al_2O_3 crystallites during the oxidation of Al overlayers. However CO titration demonstrates this coverage *does* correspond to a minimum in the density of bare Pt sites, with $\sim$30% of Pt remaining uncovered [9]. [Thicker alumina films form 3D crystallites and hence do not further reduce the number of titratable Pt sites significantly (9)]. *We thus assign this high-temperature desorption state to surface sulphate bound at the Pt–AlO_x interface.* [Desorption of chemisorbed SO_2 from the alumina surface is discounted as this occurs at significantly lower temperatures (37), while bulk aluminium sulphate is thermally stable to 1043 K.]

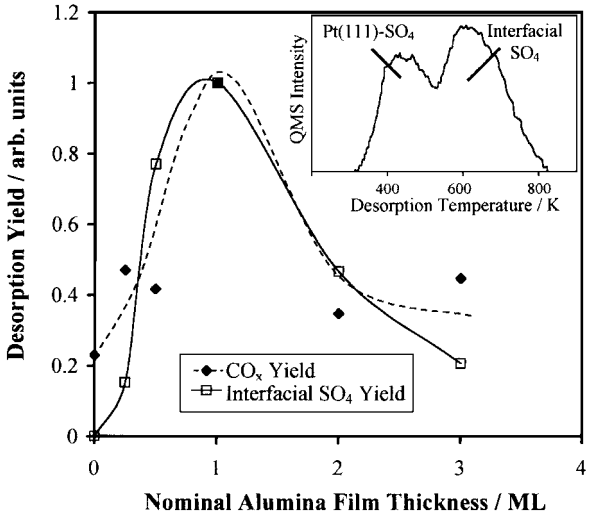

FIG. 6. Correlation between the interfacial sulphate coverage and associated catalytic combustion activity for Al_2O_3/Pt(111) surfaces as a function of alumina overlayer thickness. (Surfaces sequentially exposed to 100 L O_2 + 24 L SO_2 + 6 L C_3H_8 at 300 K.) Inset shows thermal desorption spectrum of interfacial SO_4 from a 1 ML Al_2O_3/Pt(111) film.

The intensity of this strongly bound interfacial sulphate clearly correlates with the associated combustion activity

of these sulphated Al_2O_3/Pt(111) surfaces. We suggest this interfacial sulphate species is thus more efficient at activating propane than sulphated Pt metal sites alone. The latter, however, remain essential for the dissociative chemisorption of oxygen and subsequent oxidation of alkyl fragments adsorbed both directly from the gas phase and *via* spillover from interfacial sulphate reaction centres. An interaction between platinum, sulphate, and alumina, producing high-reactivity interfacial sulphate sites, is also postulated in IR studies of dispersed Pt/Al_2O_3 catalysts (44).

CONCLUSIONS

1. At low metal loadings (~0.05 wt%) unsulphated Pt/Al_2O_3 catalysts contain principally particles of PtO_2 which are ineffective for propane oxidation.

2. Higher metal loadings correspond to the presence of metallic Pt particles and significant combustion activity. The structure sensitivity of propane oxidation is thus understandable.

3. Sulphation results in the reduction of small PtO_2 particles to Pt with partial sintering of the latter. The suppression of structure sensitive behaviour by sulphation is therefore also understandable.

4. In addition to the chemical and morphological effects noted above, sulphation acts to promote propane oxidation by facilitating the dissociative chemisorption of the alkane on the Pt surface and, especially, at the Pt/alumina interface.

REFERENCES

1. (a) Taylor, K. C., *in* "Catalysis Science and Technology" (J. R. Anderson and M. A. Boudart, Eds.), Vol. 5. Springer-Verlag, Berlin, 1984. (b) McCabe, R. W., and Kiesenyi, J. M., *Chem. Ind.* 605 (1995).
2. Sadowski, G., and Treibmann, D., *Z. Chem.* **19**, 189 (1979).
3. Yao, H. C., Stepien, H. K., and Gandhi, H. S., *J. Catal.* **67**, 237 (1981).
4. Hubbard, C. P., Otto, K., Gandhi, H. S., and Ng, K. Y. S., *J. Catal.* **144**, 484 (1993).
5. Ansell, G. P., Golunski, S. E., Hatcher, H. A., and Rajaram, R. R., *Catal. Lett.* **11**, 183 (1991).
6. Armor, J. N., *Appl. Catal. B: Env.* **1**, 221 (1992). Frost, J. C., and Smedler, G., *Catal. Today* **26**, 207 (1995).
7. Adams, K. M., Cavataio, J. V., and Hammerle, R. H., *Appl. Catal. B* **10**, 157 (1996).
8. Wilson, K., Hardacre, C., and Lambert, R. M., *J. Phys. Chem.* **99**, 13755 (1995).
9. Wilson, K., Lee, A. F., Hardacre, C., and Lambert, R. M., *J. Phys. Chem. B* **102**, 1736 (1998).
10. Horton, J. H., Moggridge, G. D., Ormerod, R. M., Kolobov, A. V., and Lambert, R. M., *Thin Solid Films* **237**, 134 (1994).
11. Hubbard, C. P., Otto, K., Gandhi, H. S., and Ng, K. Y. S., *J. Catal.* **139**, 268 (1993).
12. JCPDS File 37-1087.
13. Moselhy, H., Pokol, G., Paulik, F., Arnold, M., Kristof, J., Tomor, K., Gal, S., and Pungor, E., *J. Therm. Anal.* **39**, 595 (1993).
14. Deng, Y., and An, L., *Appl. Catal. A: Gen.* **119**, 13 (1994).
15. JCPDS File 04-0802.
16. Sham, T. K., Naftel, S. J., and Coulthard, I., *J. Appl. Phys.* **79**, 7134 (1996).
17. Bianconi, A., *in* "X-ray Absorption: Principles, Applications, Techniques of EXAFS, SEXAFS and XANES" (D. C. Koningsberger and R. Prins, Eds.). Wiley, New York, 1988.
18. Mansour, A. N., Cook, J. W., Jr., and Sayers, D. E., *J. Phys. Chem.* **88**, 2330 (1984).
19. Meitzner, G., Via, G. H., Lytle, F. W., and Sinfelt, J. H., *J. Phys. Chem.* **96**, 4960 (1992).
20. Joyner, R. W., *J. Chem. Soc., Faraday Trans. 1* **76**, 357 (1980).
21. Cheung, T. T. P., *Surf. Sci.* **140**, 151 (1984). Mason, M. G., *Phys. Rev. B* **27**, 748 (1983).
22. Vaarkamp, M., *Catal. Today* **39**, 271 (1998).
23. Borgna, A., Le Normand, F., Garetto, T., Apesteguia, C. R., and Moraweck, B., *Catal. Lett.* **13**, 175 (1992).
24. McCabe, R. W., Wong, C., and Woo, H. S., *J. Catal.* **114**, 354 (1988).
25. Hicks, R. F., Qi, H., Young, M. L., and Lee, R. G., *J. Catal.* **122**, 280 (1990).
26. Otto, K., *Langmuir* **5**, 1364 (1989).
27. Sun, Y.-M., Sloan, D., Alberas, D. J., Kovar, M., Sun, Z.-J., and White, J. M., *Surf. Sci.* **319**, 34 (1994).
28. Mordente, M. G. V., and Rochester, C. H., *J. Chem. Soc., Faraday Trans. I* **85**, 3495 (1989).
29. Barbier, J., Bahloul, D., and Marecot, P., *Catal. Lett.* **8**, 327 (1991).
30. Roberts, M. W., and McKee, C. S., *in* "Chemistry of Metal/Gas Interface." Oxford Univ. Press, Oxford, 1978.
31. Ruckenstein, E., and Chu, Y. F., *J. Catal.* **59**, 109 (1979).
32. Burch, R., and Hayes, M. J., *J. Molec. Catal. A: Chem.* **100**, 13 (1995).
33. Xu, X., and Friend, C. M., *J. Am. Chem. Soc.* **113**, 6779 (1991).
34. Otto, K., Andino, J. M., and Parks, C. L., *J. Catal.* **131**, 243 (1991).
35. Wilson, K., Hardacre, C., and Lambert, R. M., *in* "Heterogeneous Hydrocarbon Oxidation" (B. K. Warren and S. T. Oyama, Eds.), ACS Symposium Series 638. American Chemical Society, Washington, DC, 1996.
36. Firment, L. G., and Somorjai, G. A., *J. Chem. Phys.* **66**, 2901 (1977).
37. Saur, O., Bensitel, M., Saad, A. B. M., Lavalley, J. C., Tripp, C. P., and Marrow, B. A., *J. Catal.* **99**, 104 (1986).
38. Chang, J.-R., Chang, S.-L., and Lin, T.-B., *J. Catal.* **169**, 338 (1997).
39. Vaarkamp, M., Miller, J. T., Modica, F. S., Lane, G. S., and Koningsberger, D. C., *J. Catal.* **138**, 675 (1992).
40. Wilson, K., Lee, A. F., Brake, J., and Lambert, R. M., *Surf. Sci.* **387**, 257 (1997).
41. Den Otter, G. J., and Dautzenberg, F. M., *J. Catal.* **53**, 116 (1978).
42. Cairns, J. A., Baglin, J. E. E., Clark, G. J., and Ziegler, J. F., *J. Catal.* **83**, 301 (1983).
43. Wilson, K., Hardacre, C., Baddeley, C. J., Ludecke, J., Woodruff, D. P., and Lambert, R. M., *Surf. Sci.* **372**, 279 (1992).
44. Hubbard, C. P., Otto, K., Gandhi, H. S., and Ng, K. Y. S., *Catal. Lett.* **30**, 41 (1995).